Dynamics of a ball bouncing on a rough inclined line

Alexandre Valance and Daniel Bideau
Groupe Matière Condensée et Matériaux, UMR 6626, Université Rennes 1, F35042 Rennes Cedex, France
(Received 20 May 1997; revised manuscript received 12 September 1997)

We present here a simple theoretical model that describes the motion of ball bouncing on a rough inclined line. The rough line consists of microfacets whose orientation can be different from the line inclination. We examine the behavior of the ball as a function of the orientation of the microfacets and determine the conditions under which the jumps of the ball are decreasing or increasing in their amplitude. In particular we show that when the facet inclination varies along the line with a well-defined spatial periodicity the ball can reach a steady bouncing regime that leads ultimately to chaotic behavior via a period-doubling scenario. Furthermore, we find that the presence of noise associated with facet inclination destroys the structure of the chaotic regime. [S1063-651X(98)02202-8]

PACS number(s): 83.70.Fn, 46.10.+z, 46.30.Pa, 46.90.+s

I. INTRODUCTION

Despite intensive efforts in the field of granular materials [1–3], the seemingly simple problem of the dynamics of a single grain interacting with a set of boundaries is far from being completely understood. The interest for such a problem has been brought back to the fore in the mid 1980s when it had been recognized that the motion of a ball dropped onto a flat oscillating surface may give rise to chaotic behavior [4–10]. More recently, experimental works [11–13] investigating the motion of a ball rolling on an inclined rough surface have yielded interesting phenomena, which have not yet been elucidated.

In this paper we are precisely dealing with some aspects of this problem. The study of such a system can be regarded as a first step towards the understanding of the energy exchange problem between a rough substrate and an ensemble of particles, which is of crucial importance in granular flow. Within this context, numerous experimental and numerical works [11–15] already have been devoted to the study of the motion of a single sphere rolling on a rough inclined plane. It is worthwhile mentioning the main outcomes. Three different regimes have been clearly identified: (i) a decelerated regime where the velocity of ball progressively decreases until it stops, (ii) an intermediate regime where the ball reaches a steady motion with a constant velocity (the effective frictional force acting on the ball is viscous), and (iii) a jumping regime where the ball experiences big bounces and apparently does not achieve a steady state. The two first regimes have been widely explored [11–17] and are quite well understood, while the third still raises some fundamental questions.

In this paper we focus on the bouncing regime. Our aim is to analyze within a simple theoretical model the motion of a ball bouncing on a rough inclined line and to characterize carefully the role of the line roughness on the motion. In particular we are interested in determining the conditions under which the bouncing particle can reach steady regimes and whether the particle dynamics may lead to chaotic behavior in the same fashion as a bouncing ball on a vibrating plate.

The approach adopted here is inspired by that suggested by Roux and Jenkins [18]. The key point of the approach is to model the roughness of the inclined line in a very simple way. Indeed, we consider that the inclined line is made up of microfacets whose inclination is not necessarily the same as the line slope. The originality of the model is to pose a complicated problem in simple terms still preserving the essential physical ingredients. In the first stage, we will analyze the ball motion in the simple situation where all the facets have the same inclination. Then we will focus on the case where the inclination of the facets varies along the line. In particular we show that when the facet inclination has a well-defined spatial periodicity, there exists steady bouncing regimes that can destabilize and lead ultimately to chaotic dynamics via a period-doubling scenario. Furthermore, it is found that the presence of noise associated with facet inclination destroys the structure of the chaotic regime.

Our paper is organized as follows. In Sec. II we present our model in detail. In Sec. III we analyze the motion of the ball as a function of the inclination of the facets. We first treat the case where the facet inclination is assumed to be constant along the line. Then we investigate the case where the inclination of the facets varies along the line with a well-defined spatial periodicity. In Sec. IV we examine the effect of noise associated with facet inclination on the ball behavior. Section V contains the conclusion and prospects for future investigation.

II. THEORETICAL APPROACH

The rough line, on which the ball is dropped, is depicted in Fig. 1. The line forms an angle α with respect to the horizontal, while the microfacets make an angle β with respect to the inclined line. The facet inclination is not necessarily uniform, but can vary along the line. In the general case, the facet orientation is taken to be dependent of the facet position x along the line and given by the function $\mathcal{B}(\chi)$. The size of the facets is not taken into account here and is unimportant for our purpose.

Let us describe the motion of the ball on this line. At time $t=0$, the ball is launched from the position $x=x_0$ on the line with an initial velocity $\vec{V}_0$. The ball will experience successive bounces and collisions with the facets of the inclined

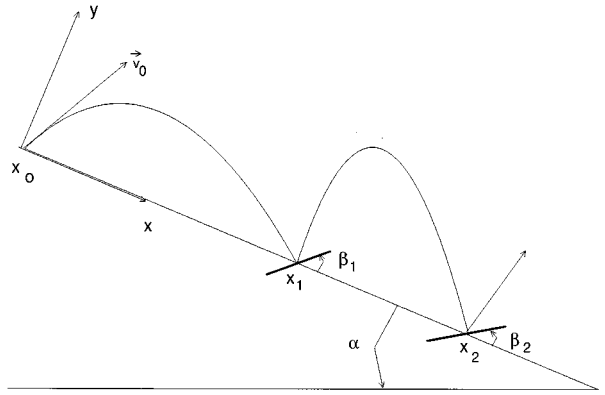

FIG. 1. Schematic view of the inclined line consisting of microfacets whose inclination β can vary according to their position. On the scheme only the facets hit by the ball have been drawn. x_i ($i=0,1,2,\ldots$) denotes the position of the successive collision impacts, while β_i is the inclination of the corresponding facets.

line. The ball motion is a repetition of elementary sequences and each sequence consists both of one ballistic bounce and one collision. To describe the ball motion, it then suffices to analyze one elementary sequence. Our aim is to find a map that relates the collision impact positions and the postcollision velocities between two successive collisions.

First we analyze the ballistic bounce. Let us call $\vec{V}_i$ the ball velocity just after the ith collision and x_i its position. The ball velocity $\vec{V}$ just before the next collision impact is easily calculated by solving Newton's equation. The calculation yields

$$V_x = V_{i,x} + 2V_{i,y}\tan\alpha, \tag{1}$$

$$V_y = -V_{i,y}. \tag{2}$$

$V_{i,x}$ and $V_{i,y}$ are the components of the velocity vector $\vec{V}_i$ along the x and y axes, respectively. We note that the velocity of the ball at the end of the bounce is independent of the gravitational acceleration. It is only a function of the initial impulse and the inclination of the line.

The duration δt_i and the length δx_i of the bounce are also easily calculated. The time t_{i+1} at which the $(i+1)$st collision occurs and its impact position x_{i+1} are simply given by

$$t_{i+1} = t_i + \delta t_i, \tag{3}$$

$$x_{i+1} = x_i + \delta x_i, \tag{4}$$

where

$$\delta t_i = \frac{2V_{i,y}}{g\cos\alpha}, \tag{5}$$

$$\delta x_i = \frac{2}{g\cos\alpha}(V_{i,x}V_{i,y} + V_{i,y}^2\tan\alpha). \tag{6}$$

g is the gravitational acceleration.

The next step is to analyze the collision of the ball with the facets of the line. After the bounce, the ball hits the facet that is located at the position x_{i+1} and whose inclination is given by $\mathcal{B}(\chi_{i+1})$. In order not to complicate the problem, we will ignore the rotation of the ball as it bounces down the line. Furthermore, we assume that after the collision the velocity components normal and tangential to the facet at the point of impact are related to the corresponding velocities before the collision by

$$V_n' = -e_n V_n, \tag{7}$$

$$V_t' = e_t V_t. \tag{8}$$

e_n (e_t) is the normal (tangential) coefficient of restitution and the prime denotes values just after the collision. Finally, the collision will be considered to be punctual (the point of contact is at rest during the collision) and the restitution coefficients to be constant (i.e., independent of the impact velocity).

Using the above collision equations, we can determine the velocity components $\vec{V}_{i+1,x}$ and $\vec{V}_{i+1,y}$ just after the $(i+1)$st collision. After some simple manipulations, we get

$$V_{i+1,x} = [e_t\cos^2\beta - e_n\sin^2\beta]V_x + [(e_t+e_n)\sin\beta\cos\beta]V_y, \tag{9}$$

$$V_{i+1,y} = [(e_t+e_n)\sin\beta\cos\beta]V_x + [(e_t\sin^2\beta - e_n\cos^2\beta)]V_y, \tag{10}$$

where β stands for the facet inclination, which is located at the position x_{i+1}, so that

$$\beta \equiv \mathcal{B}(\chi_{i+1}). \tag{11}$$

Combining these expressions with Eqs. (1) and (2) allows us to express the velocity just after the $(i+1)$st collision as a function of the velocity component just after the ith collision:

$$V_{i+1,x} = a_1(\beta)V_{i,x} + a_2(\beta)V_{i,y}, \tag{12}$$

$$V_{i+1,y} = b_1(\beta)V_{i,x} + b_2(\beta)V_{i,y}, \tag{13}$$

where

$$a_1(\beta) = e_t\cos^2\beta - e_n\sin^2\beta,$$

$$a_2(\beta) = 2\tan\alpha(e_t\cos^2\beta - e_n\sin^2\beta) - (e_t+e_n)\sin\beta\cos\beta,$$

$$b_1(\beta) = (e_t+e_n)\sin\beta\cos\beta,$$

$$b_2(\beta) = 2(e_t+e_n)\tan\alpha\sin\beta\cos\beta + e_n\cos^2\beta - e_t\sin^2\beta.$$

One should point out that, in general, the velocity map (12) and (13) is nonlinear. Indeed, the coefficients a_k and b_k depend on the velocity $\vec{V}_i$ via the parameter β [see expressions (11) and (4)].

Before proceeding further, we find it convenient to introduce the vectorial quantity $\vec{W}_i$ characterizing the ball state just after the ith collision:

$$\vec{W}_i = (x_i, \vec{V}_i), \tag{14}$$

where x_i is the impact position and $\vec{V}_i$ the postimpact velocity of the ball at the ith collision. The map that allows us to

relate the state of the ball just after the $(i+1)$st collision as a function of its state just after the ith collision can be thus formally written as

$$\vec{W}_{i+1}=\mathcal{F}(\vec{W}_i). \tag{15}$$

In the light of the above calculation, the map $\mathcal{F}$ is given by

$$x_{i+1}=f(x_i,\vec{V}_i), \tag{16}$$

$$\vec{V}_{i+1}=M(\beta)\vec{V}_i, \tag{17}$$

where

$$f\equiv x_i+\frac{2}{g\cos\alpha}(V_{i,x}V_{i,y}+V_{i,y}^2\tan\alpha), \tag{18}$$

$$\beta\equiv\mathcal{B}(x_{i+1}). \tag{19}$$

$M(\beta)$ is a 2×2 matrix whose elements are nothing but the coefficients $a_k(\beta)$ and $b_k(\beta)$ defined above [see expressions (12) and (13)]. Note that Eq. (18) simply results from expressions (4) and (6).

Finally, to determine the ball state at the nth collision given the initial state of the ball [i.e., $\vec{W}_0=(x_0,\vec{V}_0)$], it suffices to iterate n times the map $\mathcal{F}$. We formally get

$$\vec{W}_n=\underbrace{\mathcal{F}\circ\mathcal{F}\circ\cdots\circ\mathcal{F}}_{n\ times}(\vec{W}_0). \tag{20}$$

This equation completely describe the ball dynamics.

III. BALL DYNAMICS

In this section we analyze the ball motion in two particular cases. The first one is the simplest we can think of and corresponds to the situation where the facet orientation is uniform along the line. Then we will consider the case where the facet orientation varies along the line with a well-defined periodicity.

A. Facets with uniform orientation

In the particular case where the facets have the same orientation [i.e., $\mathcal{B}(\chi)=\text{const}$], the problem greatly simplifies. Indeed, the velocity map (17) becomes linear. The velocity $\vec{V}_n$ of the ball at the nth collision can therefore be expressed simply as

$$\vec{V}_n=[M(\beta)]^n\vec{V}_0. \tag{21}$$

Expression (21) allows us to calculate directly the ball velocity after n collisions. However, we should take care to analyze the state of the ball after each collision. Indeed, it may happen that for particular values of the facet inclination the ball after few bounces hits a facet with such an incidence angle that the postcollision velocity points towards the substrate delimited by the inclined line. As a result, the ball penetrates into the substrate which is clearly not reasonable. In real experiments, the ball would undergo an additional collision with the underlying substrate, which is not taken into account in our model. These undesirable situations may occur when the facet inclination β is either negative or larger than α (β is positive with respect to the trigonometric orientation). To avoid such troubles, it then suffices to restrict the range of permissible values for β. For our purpose we will therefore confine our investigation to the cases where $0<\beta<\alpha$.

In order to characterize the bouncing ball behavior, we should analyze the eigenvalues of the matrix M. If the modulus of both eigenvalues is smaller than 1, the velocity of the ball and consequently the amplitude of its bounces will decrease until it stops. On the contrary, if at least one of the eigenvalues is bigger than 1, the ball will experience bounces at higher and higher amplitude. The eigenvalues of M are easily calculated and are found to be

$$\lambda_{1,2}(\beta)=\frac{(e_n+e_t)}{2}\lambda_0(\beta)\left[1\pm\sqrt{1-\frac{4e_ne_t}{(e_n+e_t)^2\lambda_0(\beta)^2}}\right], \tag{22}$$

with

$$\lambda_0(\beta)=\sin2\beta\tan\alpha+\cos2\beta, \tag{23}$$

while the unit eigenvectors $\vec{U}_{1,2}$ are given by

$$\vec{U}_i=\cos[\theta_i(\beta)]\vec{U}_x+\sin[\theta_i(\beta)]\vec{U}_y, \tag{24}$$

where

$$\tan[\theta_i(\beta)]=[\lambda_i(\beta)-a_1(\beta)]/a_2(\beta). \tag{25}$$

$\vec{U}_x$ ($\vec{U}_y$) is the unit vector along the x direction (y direction). Note also that the β dependence of the different quantities has been explicitly indicated.

At this stage we find it worthwhile to introduce a further assumption in order to greatly simplify the algebra. We will consider that the normal restitution coefficient e_n is equal to zero. This amounts to assuming that the collision between the ball and a facet is completely inelastic in the direction perpendicular to the facet. As a result, during a collision the ball takes off again with an angle corresponding to the facet inclination. Of course, this is a drastic and rather unrealistic approximation, but it turns out that the basic results found in this limiting case can be extended to the cases where the normal restitution coefficient is nonzero [19]. We shall discuss the implications of this assumption later on.

Within the above assumption, the eigenvalues and eigenvectors of M then simply read

$$\lambda_1=e_t\lambda_0,\quad \lambda_2=0, \tag{26}$$

while the corresponding eigendirections are defined by

$$\theta_1=\beta,\quad \theta_2=\arctan[1/(\tan\beta-2\tan\alpha)]. \tag{27}$$

Several comments are in order.

(i) One can easily shown that for $\beta=\alpha/2$ the eigenvalue λ_1 reaches a maximum given by

$$\lambda_{max}=e_t/\cos\alpha. \tag{28}$$

It follows that if $\cos\alpha$ is greater than e_t, the eigenvalue λ_1 is smaller than 1 whatever the value of β. In this case, the ball

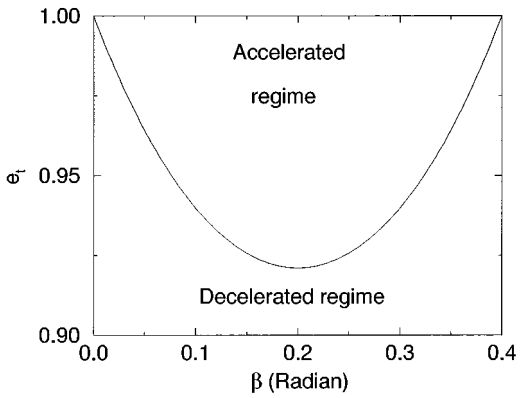

FIG. 2. Diagram showing the different regimes of the ball dynamics in the parameter space (β,e_t). The curve represents the boundary between the accelerated regime and the decelerated one. The parameter is $\alpha=0.4\simeq 23°$.

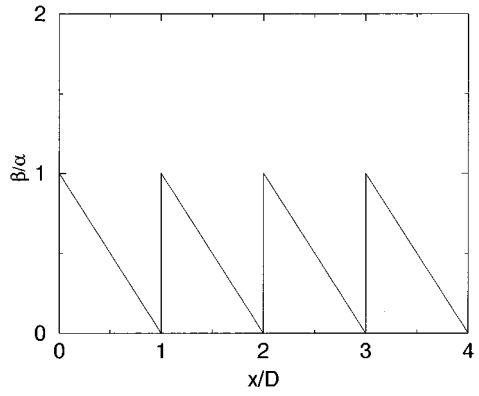

FIG. 3. Distribution of the facet orientation β as a function of their position x along the inclined line.

velocity will decrease to zero and finally stop for all β's. On the contrary, if $\cos\alpha<e_t$, there exists a finite range of values for β for which λ_1 is greater than 1. It is found that $\lambda_1>1$ for $\beta\in]\beta_0,\alpha-\beta_0[$, where β_0 and $\alpha-\beta_0$ are the critical values of β for which λ_1 is equal to 1. In the limit where e_t is close to 1, β_0 is simply given by

$$\beta_0\simeq(1-e_t)/(2\tan\alpha). \tag{29}$$

As a consequence, for $\beta_0-\alpha<\beta<\beta_0$ the ball motion is accelerated (the bounce length and amplitude will increase *ad infinitum*), whereas for $\beta\in[0,\beta_0[\cup]\alpha-\beta_0,\alpha]$ the ball will stop after several bounces. These results are synthesized in Fig. 2, which shows the domain of existence of the different regimes in the parameter space (β,e_t). The curve of Fig. 2 represents the boundary between the two regimes: below it the motion is decelerated and above it the motion is accelerated.

(ii) It can be interesting to analyze the ball motion in terms of forces acting on the ball. Using Eqs. (3), (26) and (27), it is not hard to show that after n bounces the ball velocity along the eigendirection corresponding to the nonzero eigenvalue is given by

$$(\vec{V}_n\cdot\vec{U}_1)=\sigma t_n(\vec{V}_0\cdot\vec{U}_1)+\sigma_0, \tag{30}$$

where

$$\sigma=\frac{g\cos\alpha(\lambda_1-1)}{2\cos\beta}. \tag{31}$$

σ_0 is a constant independent of t_n. If the discrete times t_n are taken to be continuous, one can rewrite the above equation in terms of forces acting on the ball

$$\frac{dv}{dt}=\sigma, \tag{32}$$

where

$$v=\vec{V}_n\cdot\vec{U}_1. \tag{33}$$

The mass of the ball has been set to $m=1$. σ can be regarded as the total force acting on the ball. This force is a compromise between the gravitational force and a frictional force due to collisions. When λ_1 is greater than 1 the gravitational force dominates, whereas for $\lambda_1<1$ the frictional force prevails. We can also note that the total force is velocity independent. As a consequence, the fictitious frictional force is thus independent of the velocity and therefore is reminiscent of the Coulomb-like frictional force. This last result can be easily understood using a straightforward argument. By virtue of the collision model used here, the energy lost per collision is quadratic in the velocity. Furthermore, the distance between two collisions is also proportional to the square of the velocity [see Eq. (6)]. Arguing that the frictional force is simply the energy lost in each collision divided by the distance between two collisions, we get a frictional force independent of the velocity. Finally, we would like to point out that if we had dropped the assumption of zero normal restitution, we would have found the same qualitative picture for the ball dynamics.

B. Facets with a spatially modulated orientation

We consider here that the facet orientation varies along the line with a well-defined spatial periodicity D. This modulation of facet orientation is intended to mimic, for example, the rough profile of a line made up of beads regularly displayed on a flat substrate. In that case D is nothing but the diameter of the beads.

For our purpose, we will assume that the distribution $\mathcal{B}(\chi)$ of the facet inclination is given by

$$\mathcal{B}(\chi)=\alpha(1-\phi), \tag{34}$$

where

$$\phi=x/D-\mathrm{Int}(x/D). \tag{35}$$

β is chosen for simplicity to be linear with x in each interval $[nD,(n+1)D]$ and to vary between 0 and α (see Fig. 3). Furthermore, the derivative of $\mathcal{B}$ with respect to x has been taken to be negative in order that the variation of facet inclination mimics the roughness of a bumpy line. We should point out, however, that with regard to a real rough profile

made up of beads, our model does not take into account the modulation of height induced by the profile of each bead.

As soon as the facet orientation is x dependent, the velocity map (17) becomes nonlinear and therefore nontrivial behavior is expected. As seen before, the ball state just after a collision is characterized by its postimpact velocity and impact position. In the specific case we are interested in, we find it more appropriate to use the parameter ϕ (defined above) instead of the impact position. This phase parameter ϕ (which varies within the interval $[0,1[$) completely characterizes the impact position. Indeed, to a value of ϕ corresponds a unique value of the facet inclination β [see Eq. (34)]. Finally, we will introduce dimensionless variables. The lengths will be reduced by the periodicity D, whereas the velocities will be reduced by $\sqrt{gD}$: $x=\overline{x}/D$ and $V=\overline{V}/\sqrt{gD}$ (the overbar denotes the variables expressed in physical units). We can rewrite the iterative map (16) and (17) in terms of the new dimensionless variables ϕ_i and $\vec{V}_i$ as

$$\phi_{i+1}=f(\phi_i,\vec{V}_i), \tag{36}$$

$$\vec{V}_{i+1}=M(\beta)\vec{V}_i, \tag{37}$$

where f and β are now given by

$$f\equiv\phi_i+\delta x_i-\mathrm{Int}(\phi_i+\delta x_i), \tag{38}$$

$$\beta\equiv\mathcal{B}(\phi_{i+1}). \tag{39}$$

$M(\beta)$ is still given by Eqs. (12) and (13). We recall that δx_i is the reduced length of the bounce next to the ith collision and is given by

$$\delta x_i=\frac{2V_{i,y}}{\cos\alpha}(V_{i,x}+V_{i,y}\tan\alpha). \tag{40}$$

We can note that in terms of dimensionless variables the iterative map $\mathcal{F}$ depends only on three parameters, namely, the line inclination α and the restitution coefficients e_n and e_t. As in Sec. III A, we will focus on the limiting case where $e_t=0$ for the sake of simplicity. In that case, given the line inclination α, the only free parameter of the problem is the restitution coefficient e_t.

Let us now analyze the ball dynamics. First we wish to determine the conditions under which the ball motion can reach a steady state. The simplest steady states we can think of are those corresponding to the fixed points of the iterative map $\mathcal{F}$. These steady states correspond to regimes where the ball experiences regular bounces: The impact positions are characterized by a unique phase parameter ϕ_s and the ball after each collision restarts with the same velocity $\vec{V}_s$ (the subscript s refers to steady states). The determination of the fixed points of $\mathcal{F}$ (which be denoted by $\vec{W}_s$ in the following) is easily achieved by taking advantage of Eqs. (36) and (37). We find that they should satisfy the conditions

$$\delta x_s=n_0, \tag{41}$$

$$\lambda_1(\beta_s)=1, \tag{42}$$

$$\vec{V}_s=V_s\vec{U}_1(\beta_s), \tag{43}$$

where n_0 is an integer and δx_s, β_s, and V_s are, respectively, the bounce length, the facet inclination (corresponding to the phase parameter ϕ_s characterizing the impact position), and the postcollision velocity of the steady state to be determined. Equation (41) just states that the length of the bounces should be a multiple of D, while Eqs. (42) and (43) simply express the fact that $\vec{V}_s$ should be a fixed point of the velocity map (37). The velocity map has fixed points only if the nonzero eigenvalue of the matrix $M(\beta_s)$ (i.e., λ_1) is equal to 1. We will see that this condition is fulfilled only for particular values of β_s (or equivalently ϕ_s).

If $e_t<\cos\alpha$, there is no steady state. Indeed, the eigenvalue $\lambda_1(\beta)$ is greater than 1 whatever the value of β. On the other hand, if $e_t>\cos\alpha$, there exist (for a given value of n_0) two steady states corresponding to the two values of β for which the eigenvalue $\lambda_1(\beta)$ is equal to 1, namely $\beta_s=\beta_0$ and $\beta_s=\alpha-\beta_0$. The use of Eqs. (41) and (43) allows us to determine V_s:

$$V_s^2=\frac{n_0\cos\alpha[1+\tan^2\beta_s]}{2\tan\beta_s[1+\tan\alpha\tan\beta_s]}. \tag{44}$$

For each of the two values of β_s, there exist an infinity of solutions associated with different values of n_0. As a result, there are two classes of steady states (corresponding to the two possible values of β_s), which will be denoted by $\vec{W}_s(\beta_s,n_0)$.

In order to know whether the system dynamics can exhibit the steady motions defined above, it is necessary to investigate their linear stability. The linear stability analysis consists in studying the regression of small fluctuations around the periodic state. Assuming that the system, initially in the steady state $\vec{W}_s$, undergoes a small perturbation $\delta\vec{W}_0$ during a collision, the ball state just after the next collision will differ from $\vec{W}_s$ and the difference will be denoted by $\delta\vec{W}_1$. After n collisions, the difference will be $\delta\vec{W}_n$. The regime will be stable if the difference $\delta\vec{W}_n$ tends to zero as n increases and it will be unstable if the difference diverges. As we are interested in small deviations from $\vec{W}_s$, we can linearize the map $\mathcal{F}$ in the vicinity of this state. $\delta\vec{W}_n$ is then linearly related to $\delta\vec{W}_{n-1}$ by

$$\delta\vec{W}_n=\frac{\partial\mathcal{F}}{\partial\vec{W}}(\vec{W}_s)\,\delta\vec{W}_{n-1}. \tag{45}$$

$\partial\mathcal{F}/\partial\vec{W}$ is a 3×3 matrix; this is the so-called Floquet or Jacobian matrix. The regime will be stable as soon as the three eigenvalues of the Floquet matrix have a modulus smaller than 1. The matrix elements are calculated analytically, whereas the determination of the eigenvalues has been performed numerically.

We have analyzed the stability of the periodic state $\vec{W}_s$ as a function of the free parameter of the problem (i.e., the restitution coefficient e_t) given the line inclination α. The calculations have been done for $\alpha=0.4\simeq23°$ and yield the following results. The steady states $\vec{W}_s(\beta_s=\alpha-\beta_0,n_0)$ are

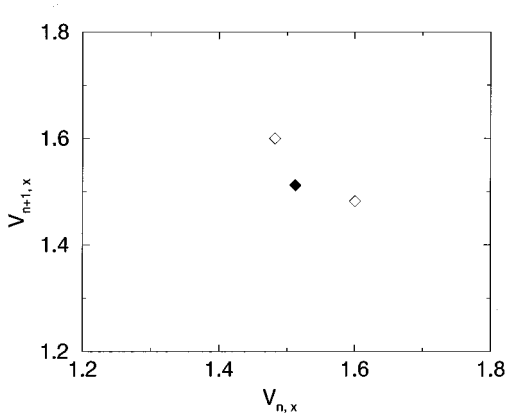

FIG. 4. Poincaré section of the ball motion: (a) the period-1 regime, filled diamond ($\alpha=0.4$ and $e_t=0.9215$); (b) the period-2 regime, open diamonds ($\alpha=0.4$ and $e_t=0.923$).

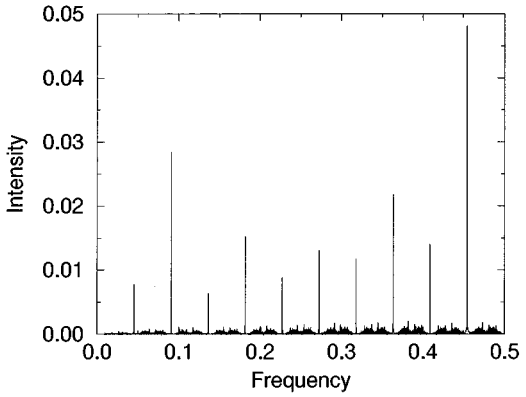

FIG. 5. Fourier transform of the postimpact velocities $V_{n,x}$ in the chaotic regime. The parameters are $\alpha=0.4$ and $e_t=0.9318$.

found to be unstable for all permissible values of e_t (i.e., $\cos\alpha<e_t<1$). The steady states of the other class [i.e., $\vec{W}_s(\beta_s=\beta_0,\ n_0)$] are also all unstable, except the one corresponding to $n_0=1$. Indeed, the steady regime associated with $\vec{W}_s(\beta_s=\beta_0,\ n_0=1)$ is found to be stable for $e_0<e_t<e_1$, where $e_0=\cos\alpha\simeq 0.9211$ and $e_1\simeq 0.9218$. This result is confirmed by computing the full ball dynamics from the map $\mathcal{F}$. The ball motion in this steady regime is illustrated in Fig. 4 in parameter space $(V_{n+1,x},V_{n,x})$. This diagram is a Poincaré section of the motion in the velocity space. Here the Poincaré section simply consists of a single spot. We will refer to this steady state as a period-p regime with a basic period $p=1$: the ball recovers periodically the same state after each collision. If the restitution coefficient is greater than e_1, the steady motion associated with $\vec{W}_s(\beta_s=\beta_0,\ n_0=1)$ becomes unstable.

The linear analysis constitutes an essential step in the analysis of the steady regimes but does not provide any information about the subsequent dynamics above the instability threshold. A nonlinear analysis, which, of course, can be only achieved numerically by computing the full ball dynamics from the map $\mathcal{F}$, is therefore needed. The computation of the ball motion reveals that above the instability threshold (i.e., $e_t>e_1$) the system undergo a period-doubling instability leading to a new steady periodic motion characterized by a basic period $p=2$. The ball recovers periodically the same state after two successive collisions (or two successive bounces). This motion is represented in Fig. 4 through the Poincaré section. One can see the apparition of a second spot indicating that the period of the motion is double what it was below the instability threshold. This period-2 state is stable as soon as $e_1<e_t<e_2$, where $e_2\simeq 0.9316$. As we increase slightly further the restitution coefficient, the ball motion undergoes a second instability, which leads to chaotic behavior. Here we do not reach the chaotic regime via the simple universal cascade of period-doubling bifurcations. In our system, the bifurcation cascade is not fully developed. The numerical analysis has not revealed period-p motions with $p=2^n$ and $n\geqslant 2$. Only the two first states of the cascade (i.e., those corresponding to $p=1$ and $p=2$) appear before the system enters the chaotic regime.

In Figs. 5 and 6 we have displayed the Fourier transform of the postimpact velocities $V_{n,x}$ and the Poincaré section of the ball motion in the chaotic regime. The Fourier transform reveals clear peaks: The first one is the basic frequency of the motion and the other one is nothing but higher harmonics. The motion is nearly periodic with a period $p=22$. The postimpact velocities visit sequentially a set of 22 distinct intervals. However, the behavior inside each interval is completely erratic, as will be seen below. We should point out here that the power spectrum does not exhibit a continuum at low frequencies as expected for a chaotic motion. This is due to the fact that we have calculated the Fourier transform of the impact velocities V_n and not that of the velocity function $V(t)$ describing the full ball motion at any time t. The chaotic feature of the motion is only clearly revealed in the Poincare map in Fig. 6. The motion attractor consists of several distinct branches suggesting the quasiperiodicity of the motion, but a careful analysis shows that each branch has a complex structure indicating the presence of a chaotic motion. Each branch exhibits self-similarity properties. Successive magnifications of the branches of the Poincaré section reveal that the same structure appears at different scales [see Figs. 6(b) and 6(c)]: Each branch is divided into two parts *ad infinitum*. We have furthermore calculated the fractal dimension, the strange attractor of which is found to be equal to $\nu\simeq 1.2$ (see Fig. 7). Other characteristics such as the Lyapunov exponents confirm the chaotic structure of the motion. If we further increase the restitution coefficient, we still observe chaotic behaviors broken with periodic motions persisting only within extremely narrow ranges of e_t. Nevertheless, above a certain value of the restitution coefficient (i.e., $e_t>0.94$), the ball motion does not possess any attractor: The ball motion becomes accelerated and the ball velocity diverges.

Our results are synthesized in Fig. 8, which shows the bifurcation diagram of the ball motion in parameter space $(e_t,V_{n,x})$. The first branch stands for the periodic motion of period $p=1$ and splits into two branches indicating the apparition of the period-2 motion. Then the period-2 state destabilizes, leading to chaos. The chaotic state is characterized by an infinite number of points: There is no more periodicity. Although these results have been obtained in the limiting case where $e_t=0$, they seem to be generic for the parameters investigated so far. For example, in the more realistic case where e_t is nonzero and $e_n=e_t$, the ball dynamics remains

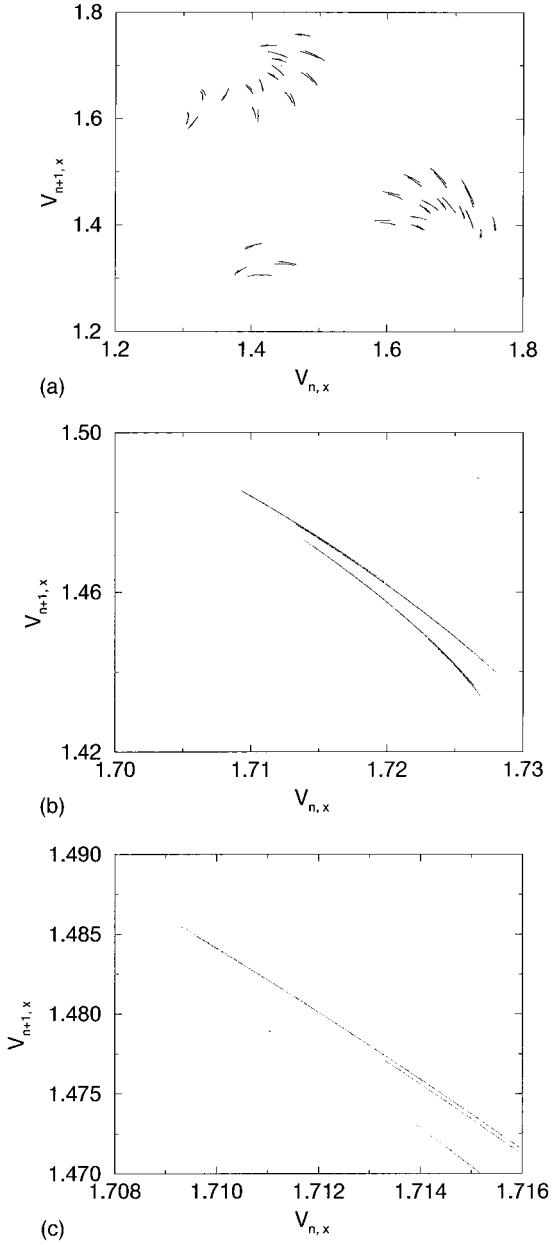

FIG. 6. (a) Poincaré section in the chaotic regime. (b) and (c) Magnifications of one branch of the attractor; the same structure appears at different scales. The parameters are $\alpha=0.4$ and $e_t=0.9318$.

qualitatively unchanged [19]: There still exists periodic motion that undergo period-doubling instabilities before leading to chaotic motion.

IV. EFFECT OF NOISE ASSOCIATED WITH FACET INCLINATION ON BALL DYNAMICS

In real experiments, the rough surface hardly exhibits a perfect spatial order. The rough surface is usually made up of beads randomly stuck on a plane substrate. The roughness therefore does not possess a well-defined spatial periodicity. So we may wonder whether the steady periodic regimes as well as the chaotic regime can persist in the presence of noise associated with facet inclination.

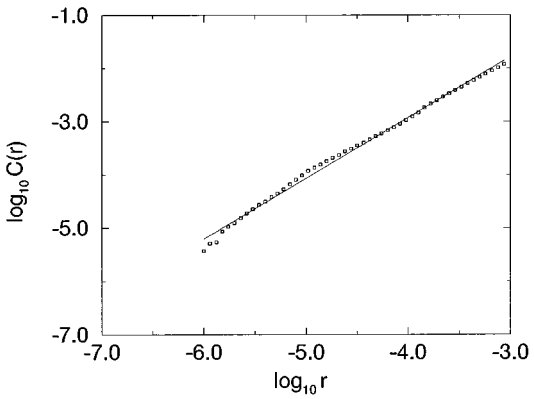

FIG. 7. Function $C(r)=\lim_{n\to\infty}(1/n^2)\Sigma_{i,j=1}^{n}H(r-|\vec{R}_i-\vec{R}_j|)$ [where $\vec{R}_i=(V_{i,x},V_{i+1,x})$ and H is the Heaviside function] calculated from the Poincaré section shown in Fig. 6(a). C obeys a power law $C(r)\sim r^{\nu}$ (where ν corresponds to the fractal dimension of the attractor). Here $\nu\simeq 1.2$. The parameters are $\alpha=0.4$ and $e_t=0.9318$.

We will consider here that the facet inclination along the inclined line is given by

$$\mathcal{B}(\phi)=\alpha(1-\phi)+\eta(\phi), \tag{46}$$

where η is a white noise term with spatially uncorrelated fluctuations

$$\langle \eta(\phi)\,\eta(\phi')\rangle=\eta_0^2\delta(\phi-\phi'). \tag{47}$$

η_0 is a mean quadratic value of the noise and can be considered as a measure of the noise strength. The distribution is intended to mimic, for example, the roughness of a surface made up of randomly spaced beads of diameter D with a spacing $D(1+\eta)$.

We examine first the incidence of the noise on the steady periodic regimes of the ball. If the noise strength is not too strong (i.e., $\eta_0<5\times10^{-2}$), the main features of the periodic motion of the ball remain qualitatively and quantitatively unchanged in comparison to the noiseless situation. Of course, as soon as stochastic noise is present in the system,

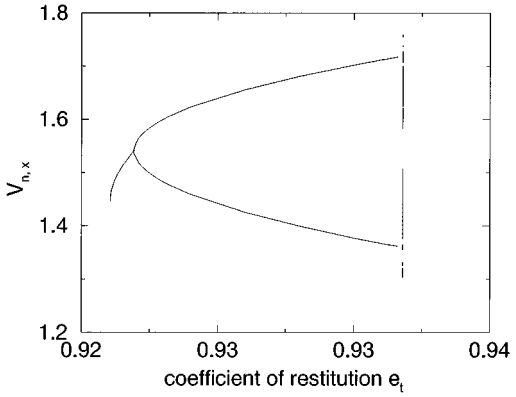

FIG. 8. Bifurcation diagram in the plane $(e_t,V_{n,x})$. In the chaotic regime, only the state corresponding to $e_t=0.9318$ has been plotted.

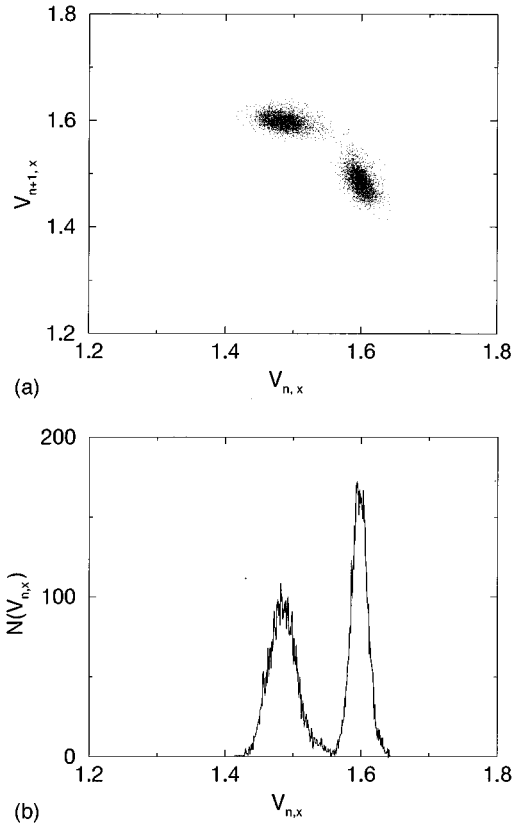

FIG. 9. (a) Poincaré section of the ball motion for $e_t=0.923$ in the presence of noise. (b) Velocity histogram of the ball motion. The parameters are $\alpha=0.4$ and $\eta_0=5\times10^{-3}$.

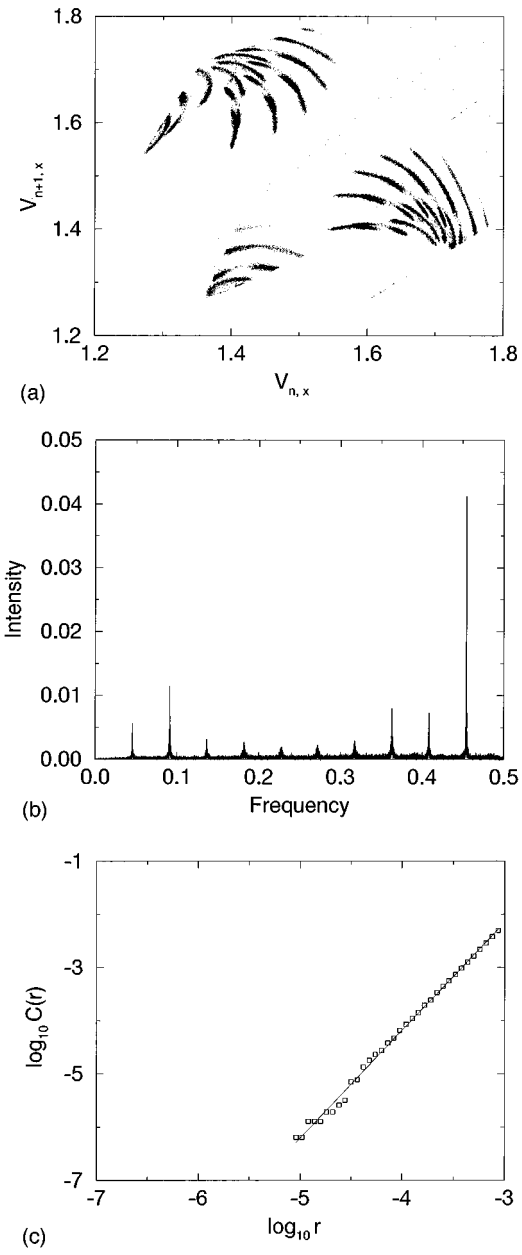

FIG. 10. (a) Poincaré section of the ball motion for $e_t=0.9318$ in the presence of noise. (b) Fourier transform of the postimpact velocities. (c) Function $C(r)$ calculated from the Poincaré section; $C(r)\sim r^{\nu}$ with $\nu\simeq2$. The parameters are $\alpha=0.4$ and $\eta_0=10^{-3}$.

one cannot observe periodic motion in a strict mathematical sense. Nevertheless, the ball motion exhibits nearly periodic features. For example, for $\eta_0=5\times10^{-3}$ and $e_t=0.923$ the ball motion [represented via the Poincaré section in Fig. 9(a)] shows similarities to the period-2 state presented in Fig. 4. The Poincaré section exhibits two spots with a finite spatial extension characterizing the dispersion around the actual period-2 regime. The dispersion around each of the two states characterizing the actual period-2 motion is found to be Gaussian as expected [see the velocity histogram Fig. 9(b)]. As one increases the noise strength, the dispersion increases, but the periodic features of the ball motion still persists. However, for strong noise ($\eta_0\geqslant10^{-1}$), the ball comes to a stop. The fluctuations are so important that the ball can leave the attraction basin of the periodic state and reach that of the rest state.

The other important point is to know whether the chaotic regime is destroyed by the presence of noise. We may naturally think that even the presence of extremely weak noise will destroy all the attributes of the chaos such as the self-similarity of the strange attractor. One surprisingly finds that the system still exhibits chaotic features for very weak noise (i.e., $\eta_0<5\times10^{-5}$). For such small values of η_0, the stochastic noise is not significant in comparison to the deterministic noise induced by the chaotic behavior. As a result, the peculiar properties of the chaotic regime (such as the self-similarity of the attractor) are preserved. The fractal dimension ν of the strange attractor is equal to 1.2, as in the case without noise. If one increases the noise strength ($\eta_0\sim10^{-4}$), one reaches a regime where stochastic noise competes with deterministic noise and then alters the chaotic features. The motion attractor still possesses self-similarity properties, but its fractal dimension ν is increased. Upon a further increase of noise intensity ($\eta_0\sim10^{-3}$), the chaotic regime is completely spoiled and loses its specific properties. Although the global structure of the attractor of the motion [Fig. 10(a)], is reminiscent of that without noise [cf. Fig. 6(a)], the attractor has completely lost its self-similarity. The ball motion still shows periodic features [see the Fourier transform in Fig. 10(b)], but the behavior inside each branch of the attractor is now purely stochastic. The points constituting each branch are randomly distributed. The dimension of the attractor is found to approach the value $\nu=2$ confirm-

ing the predominance of the stochastic noise [Fig. 10(c)]. At higher noise intensity ($\eta_0 \geqslant 10^{-1}$), the ball comes to a stop for the same reason as in the periodic regime.

As a conclusion, the deterministic chaotic regime found without noise is preserved in presence of noise only if the noise strength is extremely weak $\eta_0 \sim 10^{-5}$. In other words, this means that there is no chance to observe this chaotic regime in real experiments even with a surface made up of regularly spaced beads (where the unavoidable imperfections of the beads induces a disorder corresponding to a value of $\eta_0 \sim 10^{-3}$ in the most optimistic case). On the other hand, the different regimes observed in the absence of noise (the periodic regimes as well as the chaotic one) still exhibit periodic features in the presence of noise. One may therefore wonder whether these steady bouncing regimes can be observed experimentally. As far as we know, there has been no experimental evidence of the existence of such regimes. The nonobservation of steady bouncing regimes is, in general, attributed to the supposed long transient time and the finite length of the rough substrate used in the experiments. Within our model the transients are rather short (after about hundred bounces whose average length is of order D, the ball reaches a steady state) and therefore cannot explain that steady bouncing regimes are not seen in experiments using a 2-m-long plane made rough by sticking glass beads of diameter $D=1$ mm [13]. So we are tempted to think that the restitution coefficient of the beads used in the experiments is too high to observe steady bouncing regimes since, as mentioned before, above a critical value of e_t the ball motion accelerates. Of course, our model is very crude and in order to make conclusive comparisons with experiments, it would be strongly desired to analyze in detail more realistic situations with a nonzero normal restitution coefficient and a facet distribution that would exactly mimic a bumpy profile. This analysis is presently under study.

V. CONCLUSION

We have analyzed the dynamics of a ball bouncing on a rough inclined line within a very simple model that still retains the essential physical ingredients. In that model the rough line simply consists of facets having different orientations. Despite the simplicity of the model, it leads to nontrivial behaviors going from periodic motion to chaos. In particular when the distribution of the facet orientation exhibits a well-defined spatial periodicity along the line, the ball motion can enter a steady periodic regime that leads ultimately to a chaotic behavior via period-doubling instabilities. Furthermore, we find that the presence of stochastic noise associated with the facet orientation destroys the structure of the deterministic chaotic regime except in the case of weak noise. However, the periodic features of the ball dynamics found in the absence of noise are still revealed in the presence of noise.

A few concluding remarks should be brought to the fore. First, in the present study, we have focused on the simple limiting case where the normal restitution coefficient e_n vanishes. Although this situation is rather particular, it turns out that the basic features of the ball dynamics that we have found remain qualitatively unchanged when we release the assumption of zero normal restitution coefficient [19]. Second, the distribution of the facet orientation has been assumed to vary simply linearly with x in each interval $[nD,(n+1)D]$. We may wonder, for example, whether the ball dynamics (and the route to chaos) strongly depends on the details of the facet distribution. Moreover, it would be interesting to implement a more realistic facet distribution in order to draw conclusive answers with regard to experiments. We are presently dealing with these questions and we hope to report results in the near future.

ACKNOWLEDGMENTS

We are grateful to L. Oger and S. Roux for fruitful discussions and for a critical reading of the manuscript. We acknowledge support from the GdR CNRS ''Physique des Milieux Hétérogènes.''

[1] *Disorder and Granular Media*, edited by D. Bideau and A. Hansen (North-Holland, Amsterdam, 1993).
[2] *Granular Matter: An Interdisciplinary Approach*, edited by A. Metha (Springer-Verlag, Heidelberg, 1994).
[3] H.M. Jaeger, S.R. Nagel, and R.P. Behringer, Rev. Mod. Phys. **68**, 1259 (1996).
[4] N.B. Tufillaro and A.M. Albano, Am. J. Phys. **54**, 939 (1986).
[5] N.B. Tufillaro, T.M. Mello, Y.M. Choi, and A.M. Albano, J. Phys. (Paris) **47**, 1477 (1986).
[6] T.M. Mello and N.B. Tufillaro, Am. J. Phys. **55**, 316 (1987).
[7] A. Metha and J.M. Luck, Phys. Rev. Lett. **65**, 393 (1990).
[8] P. Boissel, Bull. Union Physiciens **86**, 217 (1992).
[9] J.M. Luck and A. Metha, Phys. Rev. E **48**, 3988 (1993).
[10] P. Devillard, J. Phys. I **4**, 1003 (1994).
[11] F.X. Riguidel, R. Julien, G. Ristow, A. Hansen, and D. Bideau, J. Phys. I **4**, 261 (1994).
[12] F.X. Riguidel, A. Hansen, and D. Bideau, Europhys. Lett. **28**, 13 (1994).
[13] G.G. Batrouni, S. Dippel, and L. Samson, Phys. Rev. E **53**, 6496 (1996).
[14] G. Ristow, F.X. Riguidel, and D. Bideau, J. Phys. I **4**, 1161 (1994).
[15] S. Dippel, G.G. Batrouni, and D.E. Wolf, Phys. Rev. E **54**, 6845 (1996).
[16] C. Henrique, M.A. Aguirre, A. Calvo, I. Ippolito, and D. Bideau, Powder Technol. (to be published).
[17] L. Samson, I. Ippolito, G.G. Batrouni, and J. Lemaitre (unpublished).
[18] S. Roux and J. Jenkins (private communication).
[19] O. Kermarrec and O. Pelhatre, Stage de Maîtrise, Université de Rennes, 1997 (unpublished).